Environmental Science
Processes & Impacts

Accepted Manuscript

ROYAL SOCIETY OF CHEMISTRY

rsc.li/process-impacts

Difference in Production Routes of Water-soluble Organic Carbon in $PM_{2.5}$ Observed During Non-Biomass and Biomass Burning Periods in Gwangju, Korea

Geun-Hye Yu[1], Sung-Yong Cho[1], Min-Suk Bae[2], Seung-Shik Park[1,*]

[1]Department of Environment and Energy Engineering, Chonnam National University, 77 Yongbong-Ro, Buk-ku, Gwangju 500-757, Korea
[2]Department of Environmental Engineering, Mokpo National University, 61 Dorim-Ri, Cheonggye-Myeon, Muan-Gun, Jeollanam-do 534-729, Korea

[*]To whom all correspondence should be addressed; phone: +82-62-530-1863; fax: +82-62-530-1859; e-mail: park8162@chonnam.ac.kr

Water-soluble organic carbon (WSOC) observed during the non-biomass burning period was mainly attributed to secondary organic aerosol (SOA). While, during the biomass burning period, there was a significant contribution of biomass burning emissions to WSOC, rather than SOA.

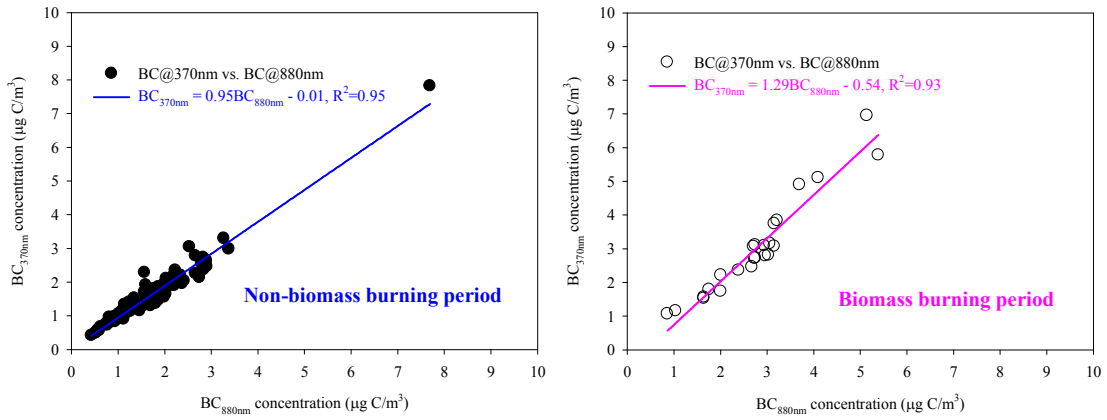

Abstract

4-hr integrated $PM_{2.5}$ samples were collected at an urban site of Gwangju, Korea, for five days and analyzed for organic carbon and elemental carbon (OC and EC), total water-soluble OC (WSOC), hydrophilic and hydrophobic WSOC fractions ($WSOC_{HPI}$ and $WSOC_{HPO}$), oxalate, and inorganic ionic species (sodium (Na^+), ammonium (NH_4^+), potassium (K^+), calcium (Ca^{2+}), magnesium (Mg^{2+}), chloride (Cl^-), nitrate (NO_3^-), and sulfate (SO_4^{2-})) to investigate the possible sources of water-soluble organic aerosols. Two types of sampling periods were classified according to the regression relationship between black carbon (BC) concentrations measured at wavelengths of 370nm (BC_{370nm}) and 880nm (BC_{880nm}) using an aethalometer; The first period was traffic emissions influences ("non-biomass burning (BB) period") and the second was biomass burning influences ("BB period"). The slope of the regression equation (BC_{370nm}/BC_{880nm}) was 0.95 for the non-BB period and 1.29 for the BB period. However, no noticeable difference in the WSOC/OC ratio, which can be used to infer the extent of secondary organic aerosol (SOA) formation, was found between the non-BB (0.61, range = 0.43-0.75) and BB (0.61, range = 0.52-0.68) periods, due to significant contribution from primary BB emissions to the WSOC. The concentrations of OC, WSOC and K^+, which were used as the BB emission markers, were 15.7 μg C/m^3 (11.5-24.3), 9.4 μg C/m^3 (7.0-12.7), and 1.2 μg/m^3 (0.6-2.7), respectively, during the BB period, and these results were approximately 1.7, 1.7, and 3.9 times higher than those during the non-BB period.

During the non-BB period, good correlations among WSOC, SO_4^{2-} and oxalate, and poor correlations among WSOC, EC, and K^+ suggest that SOA is probably an important source of WSOC (and $WSOC_{HPI}$) concentration. For the WSOC fractions, better correlations among $WSOC_{HPI}$, oxalate (R^2=0.52), and SO_4^{2-} (R^2=0.57) were found than among $WSOC_{HPO}$, oxalate (R^2=0.23), and SO_4^{2-} (R^2=0.20), suggesting that a significant proportion of the $WSOC_{HPI}$ fraction of OC could be produced through processes (gas-phase and heterogeneous oxidations) such as SOA formation. However, during the BB period, the BB emission source accounted for the high correlations between total WSOC (and WSOC fractions) and other relevant atmospheric parameters (EC, Na^+, Cl^-, K^+, and oxalate), with higher correlations in $WSOC_{HPI}$ than in $WSOC_{HPO}$. These results suggest a significant contribution of BB emissions to WSOC.

Environmental impact

Results from this study confirmed that 4-hr time-resolved measurements conducted for five days can help identify both the influences of SOA formation and biomass burning emissions to the observed WSOC. During the non-biomass burning period, a significant proportion of the hydrophilic WSOC fraction of OC could be produced through atmospheric processes such as SOA formation.

Introduction

Ambient particulate water-soluble organic carbon (WSOC) has received considerable attention due to its potential ability to influence climate radiative forcing by acting as cloud condensation nuclei.[1] Previous studies have indicated that the WSOC fraction of total OC generally tends to be lower at sites where emission sources are located, but higher in rural or background sites.[2,3] WSOC has both primary[4-6] and secondary[7] sources. Biomass burning (BB) emissions are an important primary source of WSOC in the atmosphere.[8-11] Other studies have also attributed some contributions of the observed WSOC to traffic emissions and fossil fuel combustion.[2,3,10,12-15] Cho and Park[10] attributed approximately 40% of the observed WSOC at a high traffic volume location during winter to fossil fuel emissions. Park *et al.*[15] has also shown that contributions from fossil fuel emissions to WSOC in a roadway site depend largely on changes in the dominant sources for each season, i.e., being higher in the cold season and lower in the warm season. In the absence of BB emissions, WSOC was mostly secondary.[8,13,15-18] Secondary production routes of WSOC include the atmospheric oxidation of organic species,[19] and the heterogeneous chemical reactions in cloud droplets[20,21] or haze particles.[22]

WSOC compounds can be broadly divided into hydrophilic and hydrophobic fractions.[23] The hydrophilic WSOC fraction tends to be highly water-soluble and includes compounds with low molecular weights, such as aliphatic carboxylic acids and carbonyls (<4 carbons), saccharides and amines, while the hydrophobic WSOC fraction tends to be less hygroscopic, including aliphatic carboxylic acids and carbonyls (>3-4 carbons), aromatic acids, phenols, organic nitrates, cyclic acids, and Suwannee River fulvic acids.[24] Some studies have indicated that the hydrophobic fraction of primary combustion emissions except for BB is higher than the hydrophilic fraction.[14,25,26] Other studies showed that the hydrophobic WSOC fraction in $PM_{2.5}$ made a greater contribution than the hydrophilic fraction in summer at a rural site in China[27] and an urban site in Korea,[18] probably due to further atmospheric processing during long-range transport of air masses. In addition, the hydrophobic WSOC fraction was found to be higher than the hydrophilic fraction in winter at urban sites in Korea that are impacted by both local combustion emissions and long-range transport of air pollutants from China.[14,15] However, results from another study indicate that the hydrophilic WSOC fraction with low molecular weights could be more significant during periods of active SOA production, i.e., summertime, while the hydrophobic fraction dominates during the winter in urban areas.[28] In

summary, previous studies demonstrate that the chemical features of WSOC fractions in atmospheric aerosols may depend largely on changes in the dominant sources, atmospheric aging, and the location, and that the WSOC fractions at a molecular level could provide important clues for tracking the formation pathway of organic aerosols at a specific location.

A number of studies, which discussed the composition, physical and chemical properties, sources and atmospheric transformation characteristics of organic aerosols, have been conducted around the world, but few in the region of northeastern Asia. In this study, therefore, 4-hr integrated $PM_{2.5}$ samples were collected for five days at an urban site and analyzed for OC, elemental carbon (EC), total WSOC, two WSOC fractions, oxalate, and water-soluble inorganic components. Black carbon data observed at wavelengths of 370nm and 880nm using an aethalometer were also used to classify atmospheric sampling conditions and elucidate the sources of WSOC fractions. This study aims to investigate the difference in possible sources of WSOC fractions between the non-BB and BB periods based on the classification of atmospheric conditions.

Experimental

4-hr integrated $PM_{2.5}$ measurements

$PM_{2.5}$ measurements were performed on the rooftop of a three-story building in Gwangju, Korea (latitude 35.23°N, longitude 126.85°E). A detailed description of the sampling site can be found in elsewhere.[29,30] In brief, the site is surrounded by agricultural lands and traffic roads. The closest traffic road is approximately 0.3 km from the site, and an eight-lane highway is located 1.5-2.0 km southwest of the site. There is an industrial complex located 3-8 km southwest of the site (210-250°) and a high-tech industrial area 1.0-1.5 km northeast (30-100°) of the site. Emissions from these regions to the site could be resolved during typical southwestern and northeastern flow regimes. Previous studies have shown that concentration levels of particulate matter around the site are significantly influenced by local emissions and long-range transport of air pollutants from China.[29-32] In addition, agricultural crop residues have been burned in surrounding farming areas, which are located in the direction between 290 and 60°, which enhanced the PM pollution around the site.[32-35] Meteorological data were monitored at the local automatic weather station, located 1 km south of the site.

4-hr integrated $PM_{2.5}$ samples were collected on June 07-11, 2010. Sampling started at

approximately 00:00 a.m. Aerosol samples were collected onto pre-baked (500 °C for 10 hr) quartz-fiber filters (25.4cm×20.3cm, Pall Gellman, Ann Arbor, MI) using a high-volume sampler equipped with a $PM_{2.5}$ inlet at an air flow rate of 1.13 m^3/min. Field blank samples were also collected at the beginning, the middle, and the end of the sampling period by mounting the blank filter onto the sampler for 5 minutes without sampling air. After sampling, all the samples were sealed within an aluminum foil bag and stored at -18°C prior to analysis. A non-denuded high volume sampler may adsorb gas-phase OC onto quartz filters during sampling (positive artifact).[36] However, the use of a denuder can disturb the gas/particle equilibrium at the quartz fiber filter, which can cause OC to volatilize from the filter surface (negative artifact).[36] Samples collected on the quartz filters were analyzed for OC, EC, total WSOC, two fractionated WSOC components, and ionic species. Field blanks were also analyzed to correct for background concentrations.

Concentrations of hourly OC and EC in $PM_{2.5}$ were also measured using a model-4 semi-continuous OC-EC field analyzer (Sunset Laboratory Inc., USA). This analyzer is based on the NIOSH method 5040.[37] The carbon analyzer has been described in detail elsewhere.[29] Briefly, ambient air was drawn at 8.0 l/min through a $PM_{2.5}$ sharp-cut cyclone. A carbon impregnated multi-channel parallel-plate diffusion denuder was used to prevent any semi-volatile organic vapors from absorbing on the quartz filter media. Black carbon (BC) levels were measured every 5 minutes using a seven-channel wavelength aethalometer (AE-31 model, Magee Scientific Inc.) which operated at a sampling flow rate of 5 l/min through a $PM_{2.5}$ sharp-cut cyclone.

Chemical analyses of OC, EC, total WSOC, and ionic species

The OC and EC levels in the aerosol filter samples were quantified by the NIOSH thermal-optical transmittance (TOT) standard method[37] at Sunset Laboratory Inc. (NC office, USA). Details of the OC and EC analyses are given in our previous studies.[14,18] The method detection limit (MDL) was determined as the average blank value plus three times the standard deviation of the blanks. The MDL for the OC and EC measurements was 0.48 and 0.04 μg C/m^3, respectively. The OC and EC measurement precision was 2.3 and 3.9%, respectively.

To determine the degree of equivalence, 4-hr integrated OC and EC concentrations were regressed against 4-hr averages of the 1-hr OC and EC measurements from the semi-

continuous carbon analyzer. Comparison between 4-hr averages of the 1-hr data and 4-hr filter-based data for EC and OC measurements is shown in Fig. 1. The filter-based EC concentrations were very similar to those from the semi-continuous carbon analyzer {EC_{filter} ($\mu gC/m^3$) = (1.02±0.04)EC_{semi} ($\mu gC/m^3$) + (0.03±0.20), R^2=0.96}. Filter-based OC concentrations were ~2.6 $\mu gC/m^3$ (intercept) higher than the semi-continuous OC concentrations {OC_{filter} ($\mu gC/m^3$) = (1.00±0.03)OC_{semi} ($\mu gC/m^3$) + (2.57±0.05), R^2=0.97}. The difference (offset 2.6 $\mu gC/m^3$) in the OC values was attributed to sampling artifacts between the hi-volume sampler (without the denuder) and the semi-continuous carbon analyzer (with the denuder),[29,38] to the different face velocities of air, or to the different TOT temperature programs.[39] The face velocity of air passing through the filters was 47.4 and 133.3 cm/s for the hi-volume sampler and semi-continuous carbon analyzer, respectively. Therefore, the OC data from the $PM_{2.5}$ hi-volume sampler were expected to be higher than the semi-continuous measurements.

Punches (4cm × 4cm) of the quartz fiber filter were extracted with 40 mL of ultrapure water (Barnstead Nanopure, #D11901, Thermo Scientific, USA) for two hours by ultrasonication at room temperature. The filter extracts were filtered through a syringe filter (0.45 μm). Total WSOC content was quantified using a total organic carbon analyzer (TOC, Sievers 5310C, USA) on a portion of each extract. The calculated WSOC MDL was 0.22 μg C/m^3. WSOC measurement precision was < ±5%. The TOC analysis is described in our previous studies.[14,18] The remaining portion of extract was used to separate total WSOC into hydrophilic ($WSOC_{HPI}$) and hydrophobic ($WSOC_{HPO}$) fractions using a macro-porous nonionic resin (XAD7HP) column.[14,18]

A second punch (4cm × 4cm) of each quartz fiber filter was extracted with 20 mL of ultrapure water *via* ultrasonication for 60 min to determine the concentration of water-soluble ionic species. Water extracts were filtered using a 0.45 μm membrane filter and then analyzed for eight species (sodium (Na^+), ammonium (NH_4^+), potassium (K^+), calcium (Ca^{2+}), magnesium (Mg^{2+}), chloride (Cl^-), nitrate (NO_3^-), and sulfate (SO_4^{2-})) and oxalate by ion chromatography (IC) (Metrohm 861). The determined MDL for Na^+, NH_4^+, K^+, Ca^{2+}, Mg^{2+}, Cl^-, NO_3^-, SO_4^{2-}, and oxalate was 0.18, 0.12, 0.08, 0.27, 0.04, 0.02, 0.17, 0.02, and 0.01 $\mu g/m^3$, respectively. Sample precision was 1.6, 4.3, 5.4, 0.9, 1.4, 4.7, 5.8, 5.5, and 7.7%, respectively. The IC system is discussed in the paper by Park *et al.*[18]

Hydrophilic and hydrophobic WSOC fractions

In this study, an XAD7HP (Rohm & Haas France S.A.S) column (6 mm ID × 10 cm long, Spectrum Laboratories, Inc., Houston, TX, USA) was used to group separate the total WSOC into hydrophilic and hydrophobic WSOC fractions. Detailed descriptions for pre-treatment of the used resin and the WSOC fraction separation are provided in our previous work.[18] In this study, the organic compounds which passed through the XAD7HP column were referred to as the hydrophilic fraction ($WSOC_{HPI}$), while compounds retained on the column at pH 2 were referred to as the hydrophobic components ($WSOC_{HPO}$). The column was eluted at pH 13 to recover the adsorbed hydrophobic fraction. Previous experiments indicated that the hydrophobic fractions adsorbed on the resin column are not completely recovered using a pH 13 eluent, with recovery efficiencies ranging from 75% to 85% depending on the organic compound.[24,28] Thus, the difference between total WSOC and $WSOC_{HPI}$ was defined as the $WSOC_{HPO}$ fraction. Aerosol water extracts before and after passing through the XAD column were also analyzed for eight inorganic species and oxalate using IC to check whether they were retained on the resin column. Approximately 91-100% of the water-soluble ionic species (NO_3^-, SO_4^{2-}, Na^+, NH_4^+, K^+, Ca^{2+}, Mg^{2+}, and oxalate) passed through the resin column. In this study, an average penetration efficiency of 94% for the inorganic species was applied to correct the original $WSOC_{HPI}$ concentrations. The measurement uncertainties of total WSOC and $WSOC_{HPI}$ were estimated at ±5% and ±9%, respectively.

Results and Discussion

Classification of sampling periods

In this study, the non-BB and BB sampling periods were classified based on the slope of the regression between BC concentrations measured at wavelengths of 370nm (BC_{370nm}) and 880nm (BC_{880nm}) using the aethalometer. Temporal profiles of hourly averaged BC_{370nm} and BC_{880nm} concentrations are presented in Fig. 2, along with the regression relationships between BC_{370nm} and BC_{880nm} concentrations for the non-BB and BB periods, respectively. Previous studies have used the difference in BC concentrations at wavelengths of 370 nm and 880 nm to investigate the impact of wood combustion emissions.[40,41] The impact of BB emissions on WSOC fractions was also examined from the relationship between ΔBC ($BC_{370\ nm}$ - $BC_{880\ nm}$) and WSOC, and between WSOC and estimated BB-derived BC.[15] As shown in Fig. 2(a), BC_{880nm} concentrations were higher than the BC_{370nm} concentrations with the

exception of the time periods of 22:00-00:00 on June 08 and of 16:00 on June 09 through 12:00 on June 10, suggesting impact from traffic emissions. Higher BC_{370nm} concentrations for the periods of 22:00-00:00 on June 08 and of 16:00 on June 09 through 12:00 on June 10 were due to a strong UV absorption of organic compounds in BB aerosols. The time periods when BC_{880nm} was higher and lower than the BC_{370nm} were classified as the non-BB and BB periods, respectively. Therefore, the BB period for the 4-hr integrated aerosol measurements indicates sampling periods of 20:00-00:00 on June 8 and 16:00 on June 9 – 12:00 on June 10. Regression relationships between BC_{370nm} and BC_{880nm} concentrations indicate the slope (BC_{370nm}/BC_{880nm}) of 0.95 for the non-BB period (Fig. 2(b)), which suggested the impact of traffic emissions, and of 1.29 for the BB period (Fig. 2(c)), which suggested significant impact of BB emissions on the observed aerosol samples. Kirchstetter *et al.*[42] suggested that the exponent of the wavelength dependence of light absorption for traffic-related aerosols is assumed to be equal to one for wavelengths of 370 nm and 880 nm. Some studies also indicated that certain organic aerosol components of wood burning particles have enhanced optical absorption at 370 nm relative to 880 nm.[43,44]

Fig. 3 presents temporal profiles of meteorological parameters such as wind direction, wind speed, relative humidity (RH), and ambient temperature for the entire sampling period. As seen, local winds during the first BB period (20:00-00:00 June 08) came from the northwest and northeast directions (270-55^{o}), where agricultural lands are located, with wind speeds of 1.2-2.4 m/s. During the second BB period (16:00 on June 09 – 12:00 on June 10), winds also came predominantly from the northwest and northeast directions (290-80^{o}) with wind speeds ranging from 0.4 to 3.1 m/s. Predominant wind sectors (270-80^{o}) observed during the BB periods indicate clearly that the influence of smoke from agricultural waste burning was observed at the sampling site, as evidenced by the ratio of BC_{370}/BC_{880}. BB plumes on the evening of June 8th and June 9th were observed at the agricultural lands. The RH for the BB-I and BB-II events was 66-74% and 44-75%, respectively, and ambient temperature was 17.6-20.8 and 15.6-21.6°C.

General chemical characteristics of $PM_{2.5}$

Table 1 presents summary statistics for the concentrations of the carbonaceous species and water-soluble inorganic species for the non-BB and BB sampling periods, respectively. Fig. 4 shows the temporal variation of OC, total WSOC, hydrophilic WSOC, NO_3^-, SO_4^{2-}, NH_4^+, K^+

and Cl^- concentrations for the entire sampling period. During the non-BB period, the average concentrations of EC, OC, WSOC, Cl^-, NO_3^-, SO_4^{2-}, oxalate, Na^+, NH_4^+, and K^+ were 1.39, 9.28, 5.65, 0.06, 2.49, 6.41, 0.27, 0.38, 3.10, and 0.31 μg/m^3, respectively. Their concentrations for the BB period were 2.69, 15.72, 9.43, 0.56, 4.04, 5.12, 0.33, 0.97, 3.01, and 1.20 μg/m^3, respectively. As shown in Fig. 4, NO_3^- concentrations were elevated during the nighttime due to high RH and low ambient temperature (see Fig. 3). For example, at the time period of June 8th 00:00-08:00 when the NO_3^- values of 7.11-7.27 μg/m^3 were observed, the RH and ambient temperatures were 84-93% and 16.1-18.2°C, respectively. The NO_3^- ambient concentration is strongly driven by the partitioning of nitrate between nitric acid and ammonium nitrate and boundary layer dynamics.[45] Because the RH at night was high enough to form aqueous nitric acid, the NO_3^- observed during nighttime may have accumulated in wet aerosol particles.[45,46] Thus, the increased concentrations of nighttime NO_3^- may have been related to high RH and low ambient temperatures.[29] Elevated levels of NO_3^- during the BB period were also observed. However, a study by Park *et al.*[47] performed close to our sampling site has indicated that NO_3^-, NH_4^+, and SO_4^{2-} concentrations during BB events were relatively low, accounting for only 4.0, 2.7,and 4.1% of the observed PM_{10} mass, respectively. Park *et al.*[11] has also shown that the mass fraction of NO_3^- in $PM_{1.8}$ emissions accounted for <0.4% for agricultural crop residues burns. In order to see if the enhanced NO_3^- was associated with the BB plumes, correlation analysis between the NO_3^- and K^+ was performed, giving a moderate R^2 value of 0.53 (not shown). Difference between results of this and previous studies conducted by Park *et al.*[11,47] might be due to the different biomass materials burned. High NO_3^- levels in BB plumes is also supported by another recent study by Wonaschütz *et al.*[48] Therefore, in this study, enhanced NO_3^- concentrations observed during the BB emission period were likely associated with the direct emissions from the BB. No clear variation in 4-hr integrated SO_4^{2-} concentration was observed for the non-BB and BB periods, implying contribution from long-range transported aerosols, rather than the impact of local anthropogenic and BB emissions. As shown in Fig. 4, the concentrations of K^+ and Cl^- during the BB period were obviously increased. Previous studies have reported that water-soluble K^+ and Cl^- are important inorganic components of BB emissions.[11,47-50] Park *et al.*[11] has shown that average mass fractions of K^+ and Cl^- were observed to account for 8.9 % (1.8-16.9%) and 4.9 % (3.0-9.0%), respectively, of the $PM_{1.8}$ mass emitted from agricultural crop residue burns, probably due to the application of fertilizers to paddy fields by local farmers.

Thus, the enhanced K^+ and Cl^- concentrations observed during the BB period were closely linked to agricultural practice.

Difference in production pathways of WSOC fractions between non-BB and BB periods

WSOC is mainly derived from photochemical oxidation under typical urban conditions[51] and includes highly oxygenated compounds.[16,19] In this study, the WSOC concentrations were closely correlated with the OC concentrations with a slope of 0.56 and a R^2 of 0.88 (not shown here), suggesting that these two species in the ambient air are derived from similar emission sources and/or similar formation pathways. The concentrations of WSOC during the non-BB and BB periods were 5.65 (2.98-8.67) and 9.43 (7.04-12.73) μg C/m^3, respectively. However, the average WSOC/OC ratio, which could be used to infer the extent of the secondary organic aerosol (SOA) formation, showed no difference between the non-BB and BB sampling periods, being 0.61 (range: 0.43-0.75) and 0.61 (range: 0.52-0.68), respectively. It has been suggested that the sources of WSOC include fossil fuels combustion emissions, BB, and SOA.[9,14,15,17,18,28,52] The WSOC/OC ratio in the non-BB samples was probably attributed to the gas phase and heterogeneous oxidation processes in the air, which lead to the enhancement of the SOA formation, while the WSOC/OC fraction in the BB samples was clearly due to direct emissions of agricultural waste burning, rather than to SOA production. These conclusions can be supported by a recent study conducted in Los Angeles that showed similar results for enhanced WSOC contribution to the organic fraction of aerosols in both BB plumes and transported/aged air masses.[53] Sullivan and Weber[52] have shown that in BB samples measured in an urban site dominated by summertime biogenic VOC (volatile organic compound) emissions, WSOC accounted for about 68% of the total OC. In our study, the hydrophilic and hydrophobic WSOC ($WSOC_{HPI}$ and $WSOC_{HPO}$) concentrations were 2.14 (0.60-3.96) and 3.51 (1.45-5.97) μg C/m^3 for the non-BB samples, respectively. Their concentrations were 4.02 (3.03-5.42) and 5.41 (4.01-7.31) μg C/m^3 for the BB samples, respectively. The contribution of $WSOC_{HPI}$ to total WSOC was slightly higher in the BB samples (0.43, range: 0.36-0.48) than in the non-BB samples (0.38, range: 0.11-0.54). A comparable $WSOC_{HPI}$/WSOC ratio (0.50) was also observed in BB samples analyzed in another study.[52]

Meteorological variables, such as wind speed, wind direction and weather patterns, may influence the concentrations of particulate air pollution at measurement sites. In this study,

the OC and WSOC showed negative correlations with the wind speed, with R^2 of 0.60 and 0.75, respectively (Fig. 5), indicating that local wind speed could be an important factor in controlling their concentration at the site. OC and WSOC concentrations between wind speeds of 1.0 to 3.0 m/s showed reductions of approximately 30 and 36%, respectively, indicating partially a local influence on OC and WSOC concentrations.

Correlations between the WSOC fractions and other chemical tracers were undertaken to investigate the difference of the possible sources of the fractionated WSOC between the non-BB and BB samples. The correlation analysis results for the non-BB and BB sampling periods are shown in Fig. 6 and 7, respectively. Previous studies have suggested that in the absence of BB emissions, atmospheric oxidation processes of precursor gases are a major pathway of WSOC formation.[8] More recently, however, it has been suggested that fossil fuel emissions could be an important source of WSOC observed at a roadway site and that their contribution to the fractionated WSOC varied significantly depending on the season, being higher in the cold season and lower in the warm season.[10,15] For the non-BB samples (Fig. 6), OC concentration was moderately correlated with EC concentration, which is predominantly emitted from incomplete combustion of fossil fuels, with a R^2 value of 0.52, indicating that these two components were associated with common sources, i.e., traffic emissions. However, a weak correlation was found between EC and WSOC (R^2=0.19) (Fig. 6(a)). K^+, which is a tracer of BB emissions, was also poorly correlated with OC (R^2=0.06) and WSOC (R^2=0.06) (Fig. 6(b)). The results of these correlations suggest that emissions from fossil fuel combustion and BB during the non-BB period were probably not important sources of WSOC observed at the site. To investigate whether WSOC for the non-BB period was formed as a secondary oxidation product, the relationships of total WSOC with SO_4^{2-}, NO_3^-, and NH_4^+ are shown in Fig. 6(c). The good correlations of WSOC with secondary inorganic species, SO_4^{2-} (R^2=0.63), NO_3^- (R^2=0.53), and NH_4^+ (R^2=0.55), suggest a significant contribution from secondary processes to WSOC. Fine SO_4^{2-} particles are formed by photochemical oxidation of sulfur dioxide (SO_2) and aqueous oxidation of SO_2 in clouds and fog.[45] Oxalate is predominantly produced through atmospheric processing, i.e., in-cloud or aerosol droplet processing.[54-60] and also is emitted from vehicle exhausts, fossil fuel combustion, and BB.[10,15] In this study, oxalate was poorly correlated with EC (R^2=0.03), K^+ (R^2=0.04), and NO_3^- (R^2=0.34), and well correlated with SO_4^{2-} (R^2=0.73), NH_4^+ (R^2=0.65), and WSOC (R^2= 0.64) (not shown here), suggesting secondary production of the oxalate

observed at the site. The ratio of oxalate to WSOC was also presented as a function of RH to examine the potential production pathway in the aqueous phase of the oxalate (Fig. 8). The oxalate/WSOC ratio increased with increasing the RH (R^2=0.65), indicating most likely aqueous production of oxalate. Consequently, the good correlations among WSOC, SO_4^{2-} and oxalate, and poor correlations among WSOC, EC, and K^+ suggest that the secondary processes similar to those of SO_4^{2-} and oxalate are likely production pathways of WSOC observed during the non-BB period. More specifically, for the WSOC fractions (Fig. 6 (d) and (e)), better correlations were found among $WSOC_{HPI}$, oxalate (R^2=0.52), and SO_4^{2-} (R^2=0.57) than among $WSOC_{HPO}$, oxalate (R^2=0.23), and SO_4^{2-} (R^2=0.20) during the non-BB period, suggesting that the formation processes of WSOC, exactly those of $WSOC_{HPI}$, were similar to those of oxalate and SO_4^{2-}.[15,18] In summary, a significant proportion of the $WSOC_{HPI}$ fraction of OC during the non-BB period could be produced through processes such as SOA formation.

For the BB samples, total WSOC was highly correlated with EC (R^2=0.78), K^+ (R^2=0.77), Na^+ (R^2=0.78) and Cl^- (R^2=0.90) (Fig. 7 (a)-(c)), suggesting that chemical species are closely associated with emissions from agricultural waste burning. Correlations of the secondary inorganic species to total WSOC were weak. The R^2 values for WSOC versus secondary inorganic species were 0.35 for NO_3^-, 0.08 for NH_4^+, and 0.01 for SO_4^{2-} (Fig. 7(d)). The R^2 values for the chemical species (NO_3^-, NH_4^+, SO_4^{2-}, oxalate, and EC) versus the two WSOC fractions were 0.62, 0.26, 0.04, 0.87, and 0.77 for $WSOC_{HPI}$, and 0.11, 0.01, 0.01, 0.48, and 0.55 for $WSOC_{HPO}$, respectively (not shown here). This indicates that the BB emissions were not an important factor affecting the levels of NH_4^+ and SO_4^{2-} at the site. The correlation analysis results indicate EC, WSOC (WSOC fractions), Na^+, Cl^-, K^+, and oxalate exist in $PM_{2.5}$ from BB emissions. In summary, a distinct difference was observed in the formation pathways of the WSOC fractions between the non-BB and BB periods.

Summary and Conclusion

4-hr integrated $PM_{2.5}$ samples were collected at an urban site for five days to investigate the characteristics of water-soluble organic aerosols. Two types of sampling periods, “non-BB and BB”, were classified based on the regression slope of BC concentrations measured at wavelengths of 370nm (BC_{370nm}) and 880nm (BC_{880nm}) using an aethalometer. The regression slope between the BC_{370nm} and BC_{880nm} concentrations was 0.95 during the non-BB period,

suggesting the influence of traffic emissions, while the slope was 1.29 during the BB period due to a strong UV absorption of organic compounds. WSOC during the non-BB and BB periods was mainly attributed to SOA and BB emissions, respectively. Evidence existed for an association among WSOC (and $WSOC_{HPI}$), oxalate and SO_4^{2-} concentrations during the non-BB period, indicating significant formation of SOA through cloud processing and/or an aerosol droplet process. Secondary processes can generate $WSOC_{HPI}$. However, further evidence suggested a link between WSOC ($WSOC_{HPI}$ and $WSOC_{HPO}$), EC, Na^+, Cl^-, K^+, and oxalate during the BB period.

The study results confirmed that 4-hr time-resolved measurements for 5 days can help identify both the influences of SOA formation and BB emissions to the observed WSOC. Furthermore, 4-hr time resolution permits greater resolution of emission sources than customary 24-hr integrated measurements.

Acknowledgement

This work was supported by the General Researcher Program through a NRF grant funded by the Korea government (MEST) (NRF-2011-0007222).

References

1 M.C. Facchini, M. Mircea, S. Fuzzi and R.J. Charlson, *Nature*, 1999, **401**, 257-259.
2 K.F. Ho and S.C. Lee, *Atmos. Chem. Phys.*, 2006, **6**, 4569-4576.
3 S.S. Park and S.Y. Cho, *Atmos. Environ*., 2011, **45**, 60-72.
4 R. Duarte, C.A. Pio and A.C. Duarte, *Anal. Chim. Acta.*, 2005, **530**, 7–14.
5 A. Hoffer et al., *Atmos. Chem. Phys.*, 2006, **6**, 3563–3570.
6 H. Lukacs et al., *J. Geophys. Res.*, 2007, **112**, D23S18, doi:10.1029/2006JD008151.
7 X. Zhang et al., *Geophys. Res. Lett.*, 2011, **38**, L21810, doi:10.1029/2011GL049385
8 D.C. Snyder, A.P. Rutter, R. Collins, C. Worley and J.J. Schauer, *Aerosol Sci. Technol.*, 2009, **43**, 1099-1107.
9 X. Zhang et al., *Atmos. Chem. Phys.*, 2010, **10**, 6839-6853.
10 S.Y. Cho and S.S. Park, *Environ. Sci. Processes Impacts*, 2013, **15**, 524-534.
11 S.S. Park et al., *Atmos. Environ.*, 2013, **73**, 62-72.
12 S. Ruellan and H. Cachier, *Atmos. Environ.*, 2001, **35**, 453-468.
13 A. Hecobian et al., *Atmos. Chem. Phys.*, 2010, **10**, 5965–5977.
14 S.S. Park et al., *Atmos. Environ.*, 2012, **55**, 64-72.
15 S.S. Park, J. J. Schauer and S. Y. Cho, *Atmos. Environ.*, 2013, **77**, 348-357.
16 Y. Kondo et al., *J. Geophys. Res.*, 2007, **112**, D01203, doi:10.1029/2006JD007056.
17 R.J. Weber et al., *J. Geophys. Res.*, 2007, **112**, D13302, doi:10.1029/2007JD008408.
18 S.S. Park, J.H. Kim and J.U. Jeong, *J. Environ. Monit.*, 2012, **14**, 224-232.
19 M. Kanakidou et al., *Atmos. Chem. Phys.*, 2005, **5**, 1053-1123.
20 H.J. Lim, A.G. Carlton and B.J. Turpin, *Environ. Sci. Technol.*, 2005, **38**, 4441-4446.
21 B. Ervens, B.J. Turpin and R. J. Weber, *Atmos. Chem. Phys.*, 2011, **11**, 11069–11102.

22 R. Volkamer et al., *Geophys. Res. Lett.*, 2007, **34**, L19807, doi:10.1029/2007GL030752.
23 R.M.B. Duarte and A.C. Duarte, *J. Atmos. Chem.*, 2005, **51**,79-93.
24 S.S. Park, J.U. Jeong and S.Y. Cho, *Asian J. Atmos. Environ.*, 2012, **6**, 67-72.
25 J.Z. Yu et al., *Atmos. Environ.*, 2004, **38**, 1061-1071.
26 H. Yang et al., *Atmos. Environ.*, 2005, **39**, 3735-3749.
27 Y. Miyazaki et al., *J. Geophys. Res.*, 2009, **114**, D14208, doi:10.1029/2009JD011736.
28 A.P. Sullivan and R.J. Weber, *J. Geophys. Res.*, 2006, **111**, D05314, doi:10.1029/2005JD006485.
29 S.S. Park et al., *Aerosol Air Qual. Res.*, 2013, **13**, 957-976.
30 S.S. Park et al., *Atmos. Pollut. Res.*, 2014, **5**, 119-128.
31 J. Jung, Y.J. Kim, K.Y. Lee, M.G. Cayetano, T. Batmunkh, J.H. Koo and J. Kim, *Atmos. Chem. Phys.*, 2010, **10**, 5391-5408.
32 J. Jung and Y.J. Kim, *J. Geophys. Res.*, 2011, **116**, D02206.
33 S.Y. Ryu et al., *J. Air Waste Manage. Assoc.*, 2004, **54**, 1124-1137.
34 S.Y. Ryu et al., *Atmos. Res.*, 2007, **84**, 362-373.
35 S.S. Park, M.-S. Bae, J.J. Schauer, Y.J. Kim, S.Y. Cho and S.J. Kim, *Atmos. Environ.*, 2006, **40**, 4182-4198.
36 B.J. Turpin, P. Saxena and E. Andrews, *Atmos. Environ.*, 2010, **34**, 2983-3013.
37 National Institute of Occupational Safety and Health (NIOSH), *Method 5040 Issue 1: Elemental Carbon (Diesel Exhaust)*, NIOSH Manual of Analytical Methods, Cincinnati, 4th ed., 1996.
38 R. Subramanian, A.Y. Khlystov, J.C. Cabada and A.L. Robinson, *Aerosol Sci. Technol.*, 2004, **38**, 27-48.
39 J.J. Schauer et al., *Environ. Sci. Technol.*, 2003, **37**, 993–1001.
40 C. Wu et al., *Sci. Total Environ.*, 2007, **386**, 42-52.
41 Y. Wang, P.K. Hopke, O.V. Rattigan and Y. Zhu, *J. Environ. Monit.*, 2011, **13**, 1919-1926.
42 T.W. Kirchstetter, T. Novakov and P.V. Hobbs, *J. Geophys. Res.*, 2004, **109**, D21208, doi:10.1029/2004JD04999.
43 C.H. Jeong, P.K. Hopke, E. Kim and D.W. Lee, *Atmos. Environ.*, 2004, 38, 5193–204.
44 J. Sandradewi et al., *Atmos. Environ.*, 2008, **42**, 101–112.
45 Seinfeld, J. H., Pandis, S.N., 2006. Atmospheric Chemistry and Physics: From Air Pollution to Climate Change, 2nd Ed., John Wiley & Sons, Inc., Hoboken, N.J.
46 S.S. Park, J.M. Ondov, D. Harrison and N.P.V. Nair, *Atmos. Environ.*, 2005, **39**, 2011-2020.
47 S.S. Park, S.B. Hong, Y.G. Jung and J.H. Lee, *Atmos. Environ.*, 2004, **38**, 293-304.
48 A. Wonaschütz, S.P. Hersey, A. Sorooshian, J.S. Craven, A.R. Metcalf, R.C. Flagan and J.H. Seinfeld, *Atmos. Chem. Phys.*, 2011, **11**, 8257-8270.
49 S.Q. Turn et al., *J. Geophys. Res.*, 1997, **102**, 3683-3699.
50 M.D. Hays et al., *Atmos. Environ.*, 2005, **39**, 6747–6764.
51 R.K. Pathak et al., *Atmos. Environ.*, 2011, **45**, 318-325.
52 A.P. Sullivan and R.J. Weber, *J. Geophys. Res.*, 2006, **111**, D05315, doi:10.1029/2005JD006486.
53 H.T. Duong, A. Sorooshian, J.S. Craven, S.P. Hersey, A.R. Metcalf, X. Zhang, R.J. Weber, H. Jonsson, R.C. Flagan and J.H. Seinfeld, *J. Geophys. Res.*, 2011, **116**, D00V04, doi:10.1029/2011JD016674.
54 K. Crahan, D. Hegg, D.S. Covert and H. Jonsson, *Atmos. Environ.*, 2004, **38**, 3757-3764.
55 J.Z. Yu, X.F. Huang, J. Xu and M. Hu, *Environ. Sci. Technol.*, 2005. **39**, 128-133.
56 A. Sorooshian, V. Varutbangkul, F.J. Brechtel, B. Evens, G. Feingold, R. Bahreini, S.M. Murphy, J.S. Holloway, E.L. atlas, G. Buzorius, H. Jonsson, R.C. Flagan and J.H. Seinfeld,

494 *J. Geophys. Res.*, 2006, **111**, D23S45, doi:10.1029/2005JD006880.
495 57 G. Wang et al., *J. Geophys. Res.*, 2009, **114**, D19208, dio.10.1029/2008JD011390.
496 58 S. Guo, M. Hu, Z.B. Wang, J. Slanina and Y.L. Zhao, *Atmos. Chem. Phys.*, 2010, **10**, 947-
497 959.
498 59 B. Laongsri and R.M. Harrison, *Atmos. Environ.*, 2013, **71**, 319-326.
499 60 J.-S. Youn et al., *Geophys. Res. Lett.*, 2013, **40**, doi:10.1002/GRL50644.
500
501
502

Table 1 Concentrations of carbonaceous aerosols and water-soluble inorganic components in $PM_{2.5}$ during the non-biomass burning (BB) and BB periods

		Non-BB period		BB period	
	Unit	Avg±std	Range	Avg±std	Range
EC	μg C/m^3	1.39±0.51	0.47-2.80	2.69±0.70	2.19-4.01
OC	μg C/m^3	9.28±1.93	5.42-12.98	15.72±4.47	11.48-24.34
WSOC	μg C/m^3	5.65±1.53	2.98-8.67	9.43±1.86	7.04-12.73
$WSOC_{HPI}$	μg C/m^3	2.14±0.95	0.60-3.96	4.02±0.91	3.03-5.42
$WSOC_{HPO}$	μg C/m^3	3.51±1.14	1.45-5.97	5.41±1.14	4.01-7.31
WSOC/OC	-	0.61±0.08	0.43-0.75	0.61±0.05	0.52-0.68
$WSOC_{HPI}$/WSOC	-	0.38±0.13	0.11-0.54	0.43±0.05	0.36-0.48
Na^+	μg/m^3	0.38±0.17	0.05-0.78	0.97±0.12	0.84-1.16
NH_4^+	μg/m^3	3.10±1.30	1.37-5.97	3.01±1.29	1.92-5.49
K^+	μg/m^3	0.31±0.14	0.13-0.63	1.20±0.82	0.64-2.74
Ca^{2+}	μg/m^3	0.67±0.26	0.19-1.41	1.02±0.32	0.49-1.37
Mg^{2+}	μg/m^3	0.06±0.05	0.00-0.20	0.04±0.02	0.02-0.07
Cl^-	μg/m^3	0.06±0.06	0.02-0.21	0.56±0.21	0.26-0.88
NO_3^-	μg/m^3	2.49±2.42	0.14-7.54	4.04±2.78	1.46-8.39
SO_4^{2-}	μg/m^3	6.41±1.05	4.33-8.38	5.12±1.42	3.88-7.89
Oxalate	μg/m^3	0.27±0.06	0.17-0.37	0.33±0.08	0.23-0.45

List of Figure Captions

Fig. 1 Comparison of EC and OC concentrations between the semi-continuous carbon monitor and filter-based measurements

Fig. 2 (a) Temporal profiles of BC concentration (at 370 and 880nm) and relationships between BC concentrations at 370 and 880nm for the non-BB period (b) and the BB period (c)

Fig. 3 Temporal profiles of meteorological parameters

Fig. 4 Temporal profiles of (a) OC, WSOC, and hydrophilic WSOC, (b) NO_3^-, SO_4^{2-}, and NH_4^+, and (c) K^+ and Cl^- concentrations

Fig. 5 Variation of OC and WSOC concentrations with wind speed

Fig. 6 Comparisons between WSOC fractions and other atmospheric parameters for the non-biomass burning period

Fig. 7 Comparisons between WSOC fractions and other atmospheric parameters for the biomass burning period

Fig. 8 Influence of RH on the ratio of oxalate to WSOC during the non-BB period

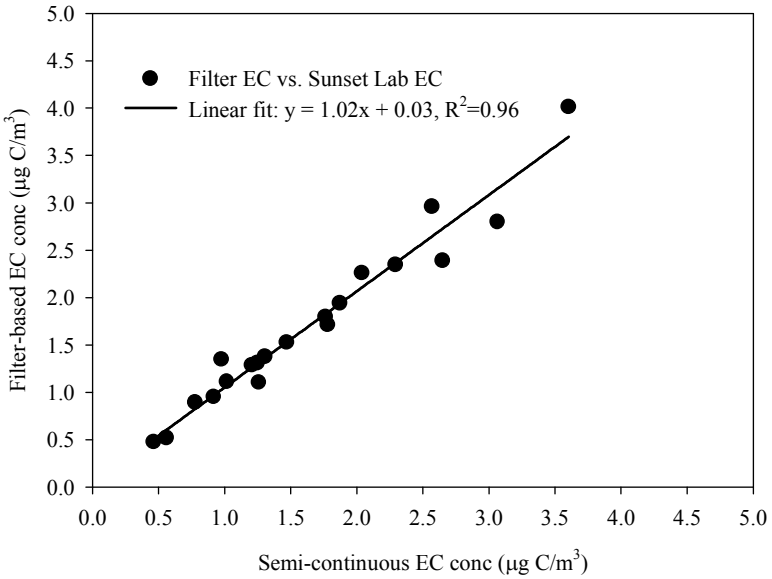

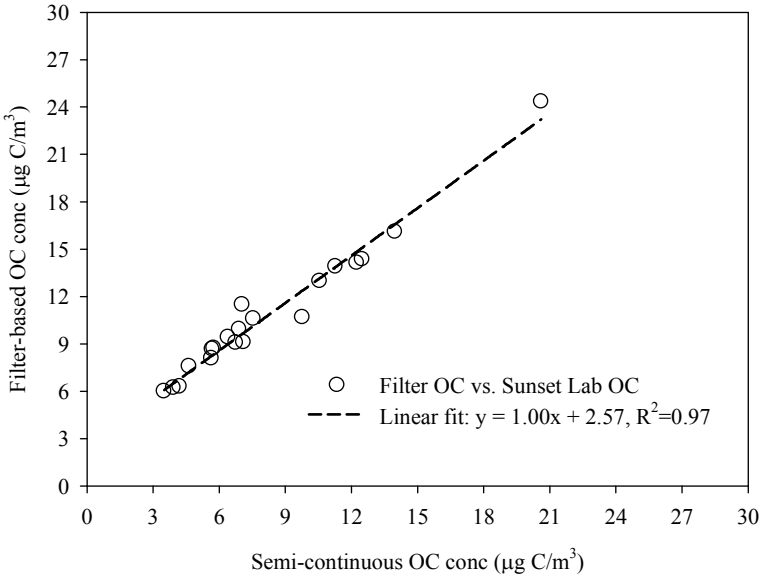

Fig. 1 Comparison of EC and OC concentrations between the semi-continuous carbon monitor and filter-based measurements

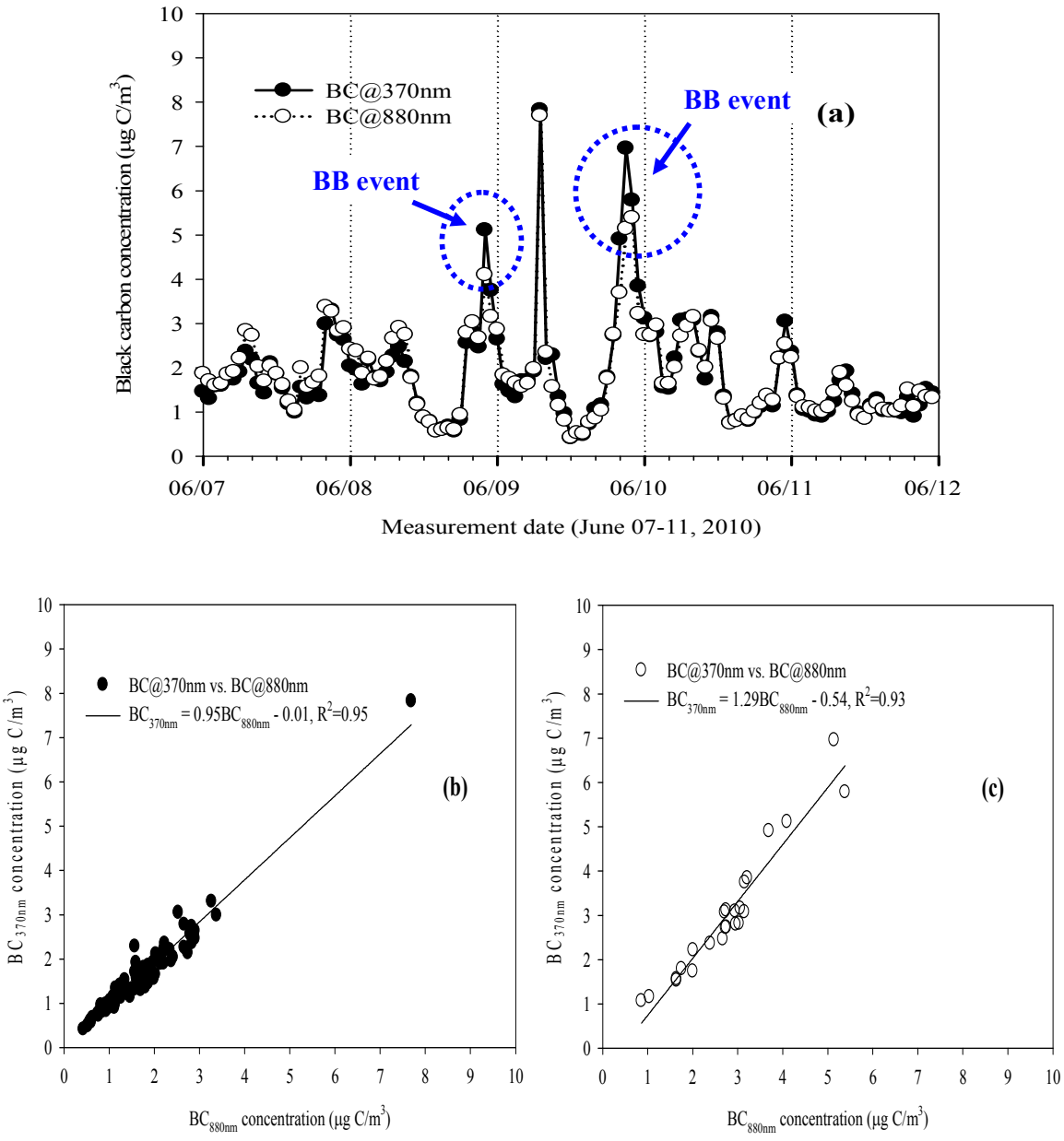

Fig. 2 (a) Temporal profiles of BC concentration (at 370 and 880nm) and relationships between BC concentrations at 370 and 880nm for the non-BB period (b) and the BB period (c)

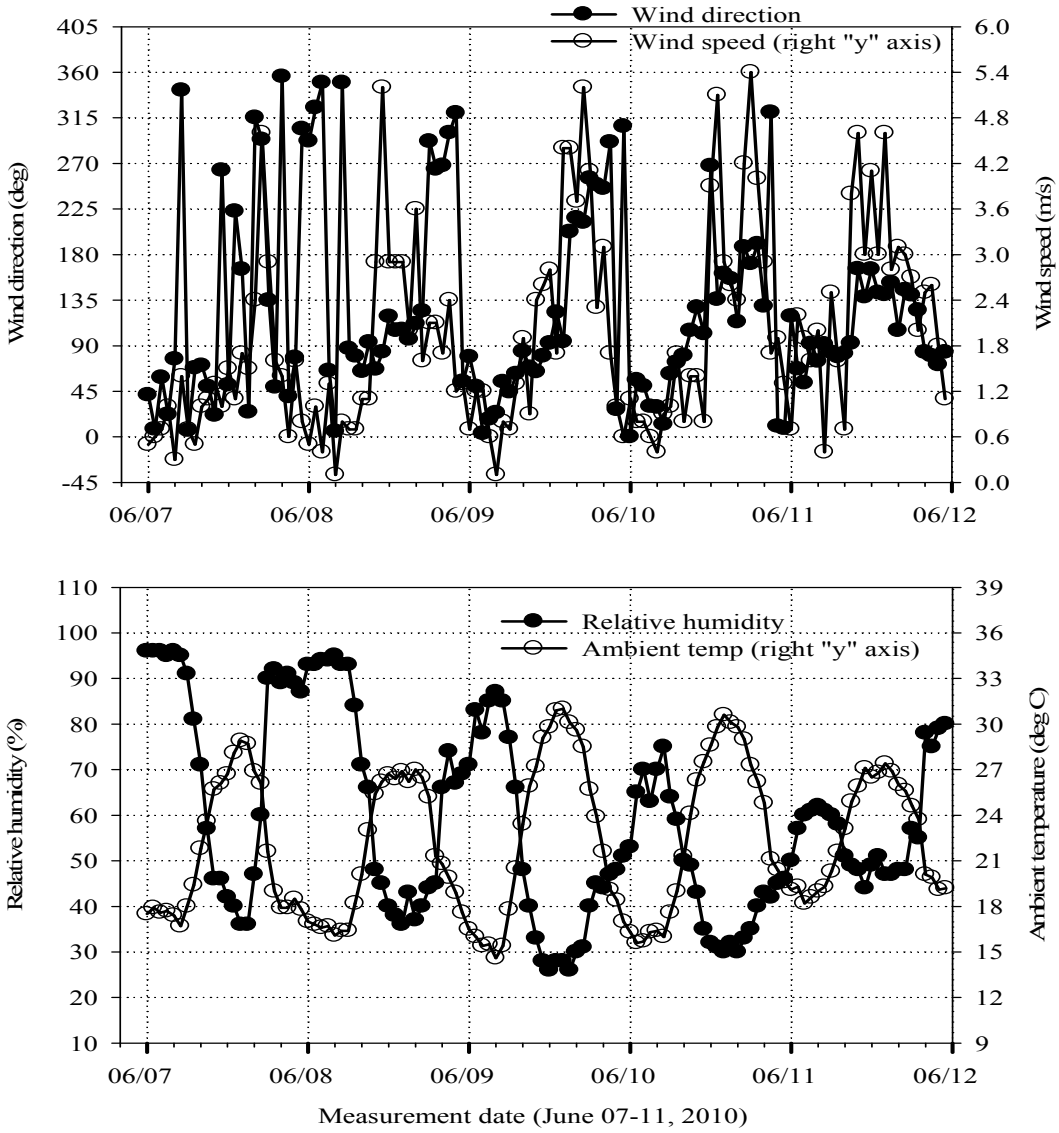

Fig. 3 Temporal profiles of meteorological parameters

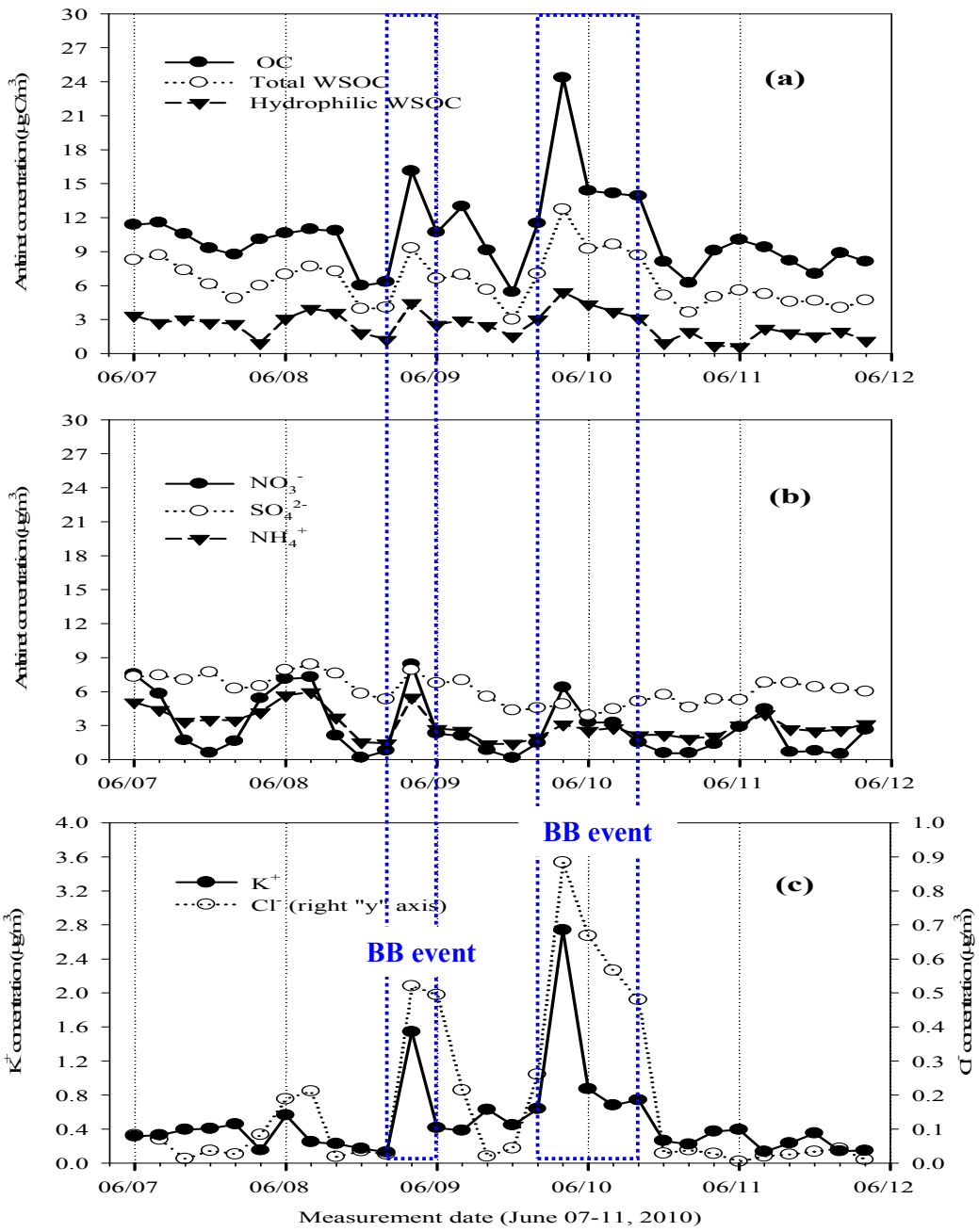

Fig. 4 Temporal profiles of (a) OC, WSOC, and hydrophilic WSOC, (b) NO_3^-, SO_4^{2-}, and NH_4^+, and (c) K^+ and Cl^- concentrations

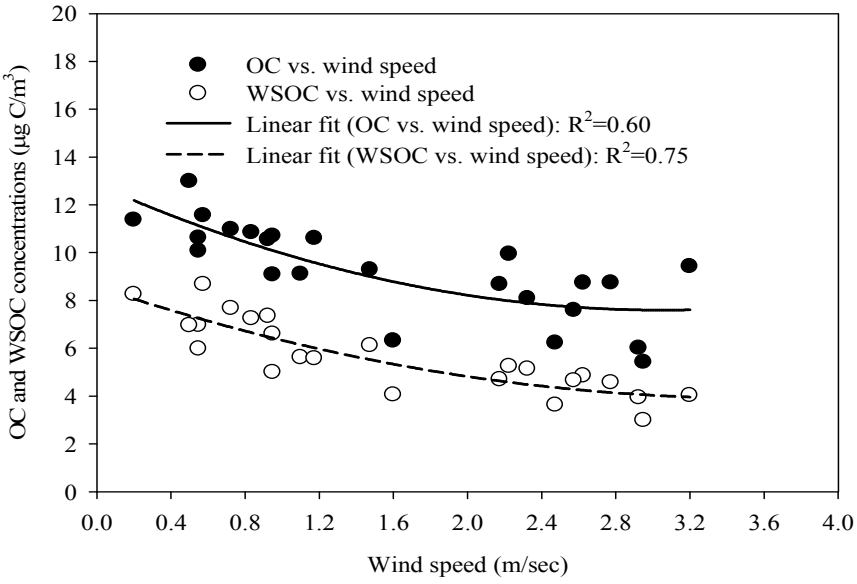

Fig. 5 Variation of OC and WSOC concentrations with wind speed

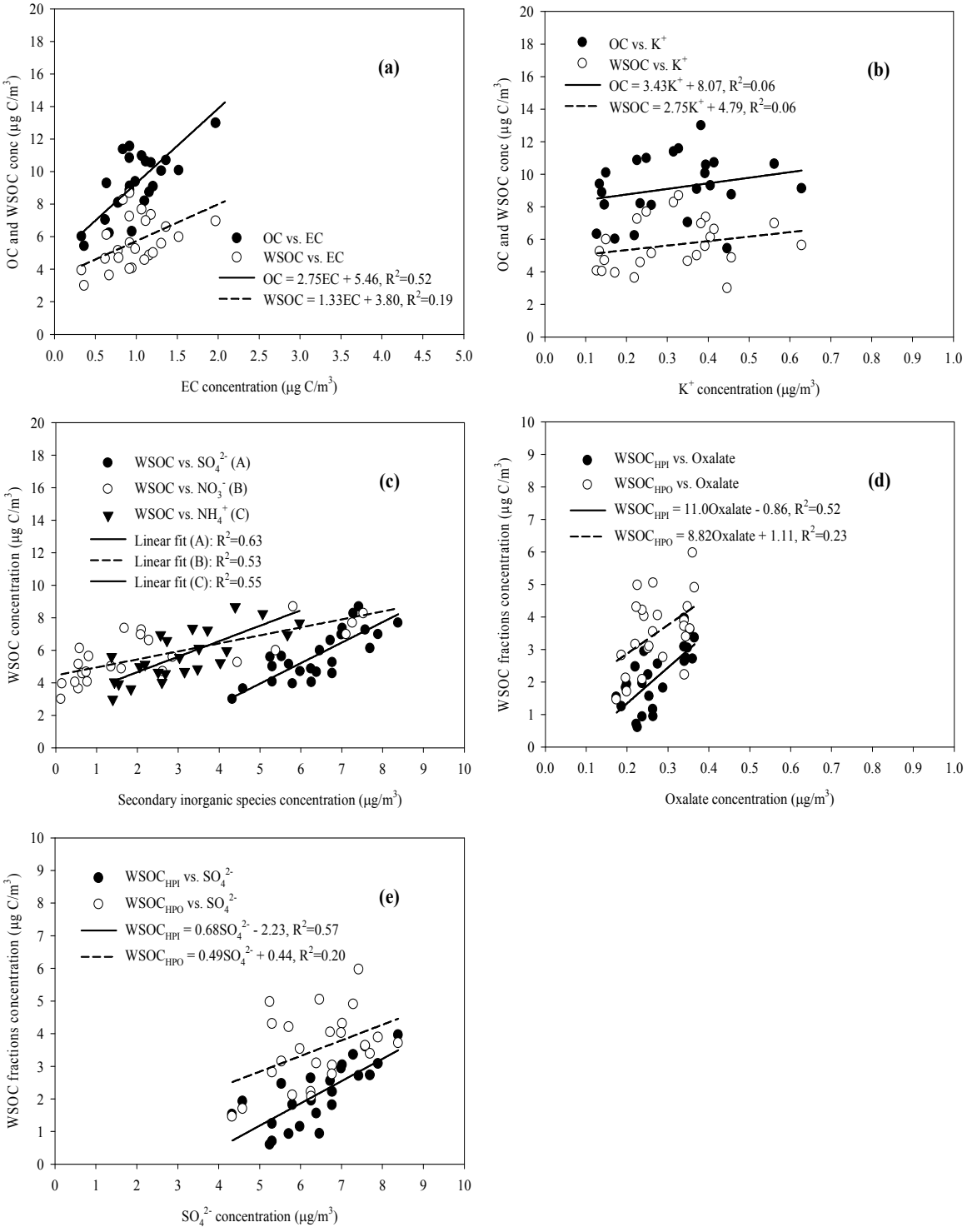

Fig. 6 Comparisons between WSOC fractions and other atmospheric parameters for the non-biomass burning period

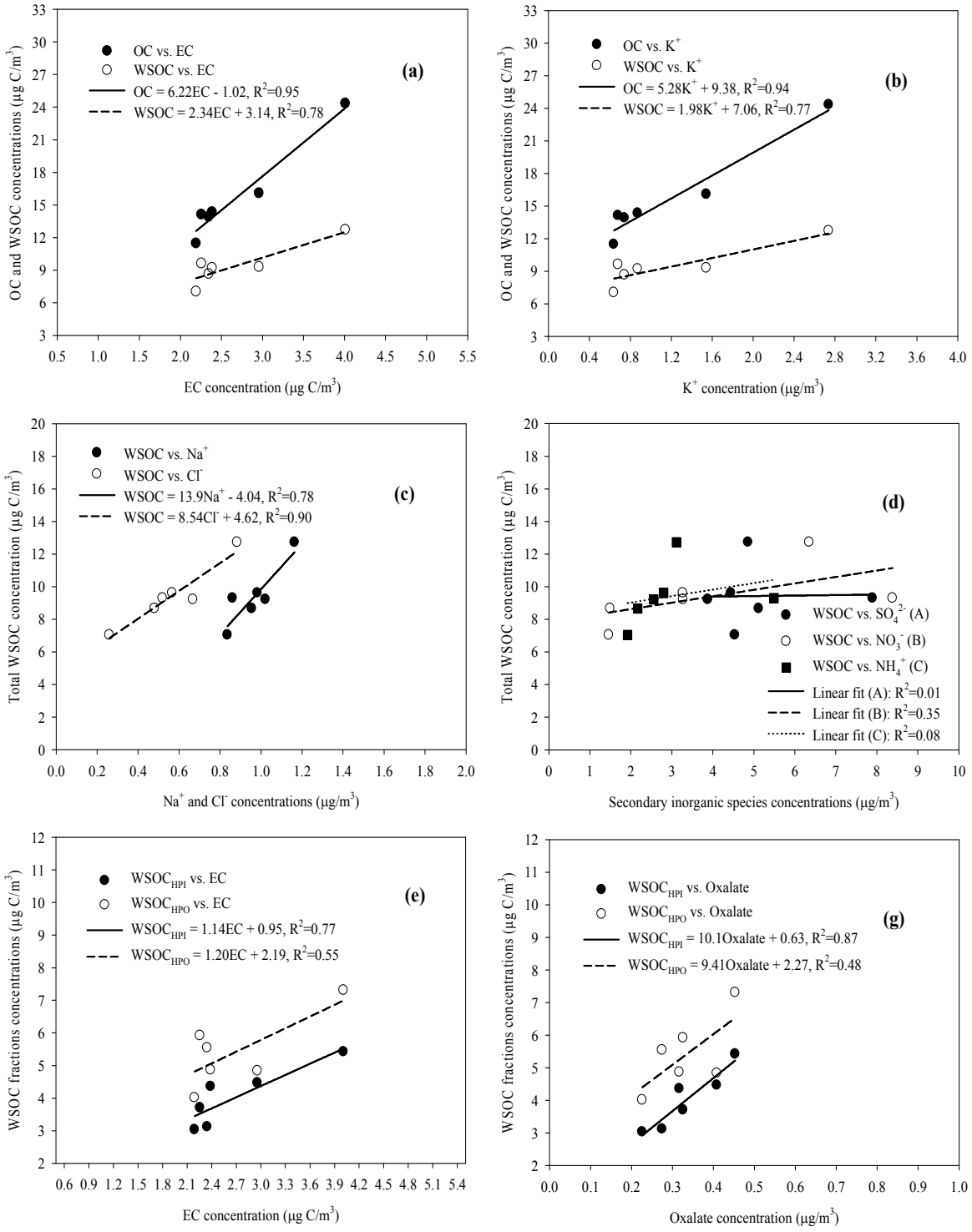

Fig. 7 Comparisons between WSOC fractions and other atmospheric parameters for the biomass burning period

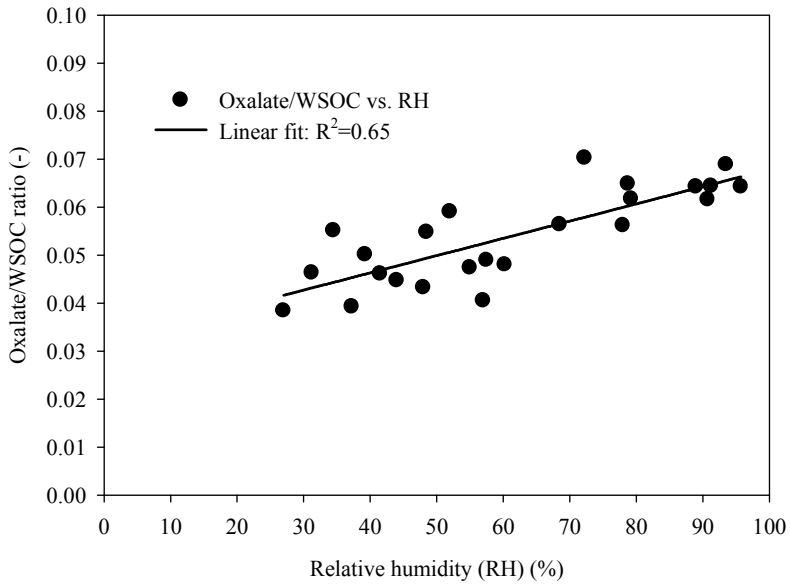

Fig. 8 Influence of RH on the ratio of oxalate to WSOC during the non-BB period